

## All Optical Waveguiding in a Coherent Atomic Rubidium Vapor

Praveen K. Vudyaasetu, David J. Starling, and John C. Howell

*Department of Physics and Astronomy, University of Rochester, Rochester, New York 14627, USA\**

(Received 10 December 2008; published 26 March 2009)

We demonstrate an all optical waveguide imprinted by a low power Laguerre Gaussian control laser beam using a coherent Raman process in warm atomic rubidium vapor. We show that the signal beam propagates with a small spot size over several diffraction lengths. We also show that the coupling efficiency of the signal beam into the waveguide varies linearly with the signal power.

DOI: 10.1103/PhysRevLett.102.123602

PACS numbers: 42.50.Gy, 42.65.An, 42.65.Jx, 42.65.Wi

Nonlinear optical properties of various gases within an optical waveguide structure have received considerable recent attention [1,2]. The use of an optical waveguide enables one to have high intensities at lower optical powers over distances much greater than the diffraction length. The combination of higher intensities, longer interaction lengths, and higher atomic densities within the mode volume results in efficient nonlinear processes [1]. Benabid *et al.* demonstrated an efficient stimulated Raman scattering process in a hollow-core photonic crystal fiber filled with hydrogen gas requiring 2 orders of magnitude less control beam power than any other previously reported experiments [1]. Efficient nonlinear processes have been demonstrated by injecting rubidium vapor in such a waveguide [2] and also by using the small optical mode area of a tapered nanofiber placed in rubidium vapor [3].

An all optical waveguide refers to a waveguide whose transverse refractive index profile is set by the interaction of an optical control beam with the medium. The properties of the waveguide can be altered or modified to fit a particular experimental requirement simply by changing the properties of the control beam. Several schemes have been proposed to achieve all optical waveguiding, and there have been some experimental realizations. Moseley *et al.* have proposed [4] and realized [5] focusing and defocusing of the signal beam using electromagnetically induced focusing. There are several other papers which address Raman focusing [6–9]. Truscott *et al.* have achieved optical waveguiding [10], and their scheme is analyzed in detail by Kapoor *et al.* [11] and Anderson *et al.* [12]. In this scheme the control beam modifies the refractive index of the medium by pumping the ground state rubidium atoms to an excited state. There are several other schemes proposed for waveguiding [13], and more recently image guiding [14], using electromagnetically induced transparency in lambda and double lambda systems.

In this Letter, we present the experimental results demonstrating the waveguiding effect in warm rubidium vapor using an off-resonance Raman transition. The transmission of the signal beam changes sharply when its frequency is near Raman resonance with the control beam. This results in changes in the refractive index at signal frequencies

around Raman resonance [15,16]. We use a donut shaped first order Laguerre Gaussian ( $LG_{01}$ ) control beam to imprint a waveguide in the atomic rubidium vapor. The refractive index at the annulus of the donut control beam is lower than that at the core for signal frequencies tuned to the blue of Raman resonance.

The experimental setup shown in Fig. 1 consists of a 795 nm external cavity tunable diode laser followed by a tapered amplifier. The beam is split in two at a 50/50 beam

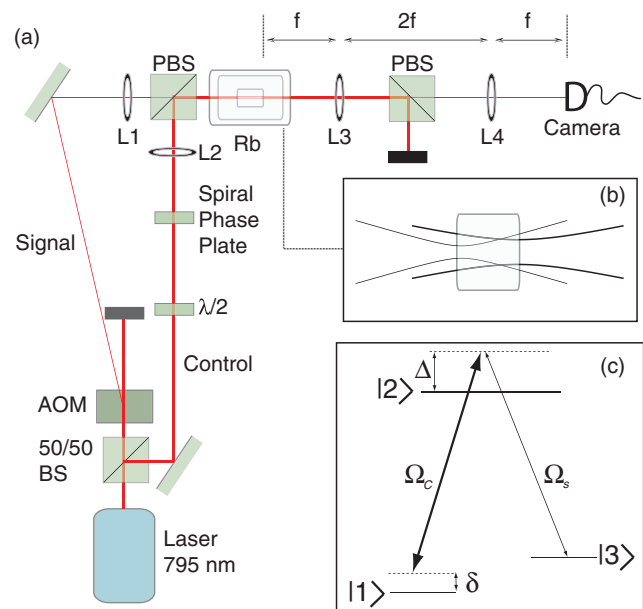


FIG. 1 (color online). (a) The experimental schematic for all optical waveguiding using atomic rubidium vapor. (b) The focusing scheme for control beam (black) and signal (gray). (c) The energy level diagram. We have a positive single photon detuning,  $\Delta$ , of about 500 MHz. Note that according to our convention positive Raman detuning is to the red of Raman resonance frequency. The waveguide is imprinted onto the rubidium atoms by a Laguerre Gaussian control beam. The signal is focused into the core of the control beam at the front of the cell. We measure the beam diameters at the back face of the cell to demonstrate guiding by imaging the back face of the cell onto the camera using the lenses  $L3$  and  $L4$  in a  $4f$  imaging configuration.

splitter. One beam acts as the signal after frequency shifting it by about 3.035 GHz to the red by double passing it through a 1.5 GHz acousto-optic modulator (AOM). The other beam acts as the control beam which is sent through a spatial filter in order to clean up its mode and is followed by a charge one spiral phase plate, resulting in a first order Laguerre Gaussian beam. The orthogonally polarized control and signal are then combined at a polarizing beam splitter (PBS). We use a configuration where the control focuses at the back face and the signal focuses into the core of the donut control beam at the front face of the vapor cell. The control is filtered at another polarizing beam splitter after the cell. We image the back face of the cell with a  $4f$  imaging system to determine the size of the signal. The antireflection coated vapor cell is 5 cm long and contains a natural abundance of rubidium isotopes with a 20 torr neon buffer gas. The vapor cell is placed inside a magnetically shielded oven and is maintained at a temperature of about 80 °C, which results in number densities of approximately  $10^{12} \text{ cm}^{-3}$ .

The experimental parameters are chosen such that the core of the LG beam has a higher refractive index than the annulus of the beam. For a lambda system the susceptibility at the signal frequency is given by [16]

$$\chi(\Omega_c, \delta, \Delta) = \frac{N\mu^2}{\hbar\epsilon_0} \frac{\delta + i\gamma}{(\delta + i\gamma)(\Delta + i\Gamma) - \Omega_c^2/4}, \quad (1)$$

where  $\Gamma$  is the excited state decay rate,  $\gamma$  is ground state decoherence rate, and  $\Delta$  and  $\delta$  are the single photon and two photon detunings, respectively. The real part of the susceptibility is given by

$$\chi'(\Omega_c, \delta, \Delta) = \frac{N\mu^2}{\hbar\epsilon_0} \frac{\Delta - \frac{\Omega_c^2}{4(\delta^2 + \gamma^2)}\delta}{(\Delta - \frac{\Omega_c^2}{4(\delta^2 + \gamma^2)}\delta)^2 + (\Gamma + \frac{\Omega_c^2}{4(\delta^2 + \gamma^2)}\gamma)^2}. \quad (2)$$

One can observe from Eq. (2) that the variation of  $\chi'(\Omega_c, \delta, \Delta)$  versus control beam Rabi frequency has the form of dispersion near a homogeneously broadened spectral line. Figure 2 depicts this behavior for various combinations of  $\Delta$  and  $\delta$ . We note that the refractive index for zero  $\Omega_c$  depends on the magnitude and sign of  $\Delta$  and the number density. When there is no control beam,

$$\chi'(\Omega_c, \delta, \Delta) = \frac{N\mu^2}{\hbar\epsilon_0} \frac{1}{\Delta}. \quad (3)$$

We also see that for all combinations of parameters,  $\chi'(\Omega_c, \delta, \Delta)$  approaches zero for very large  $\Omega_c$ . The real part of susceptibility for large  $\Omega_c$  can be approximated as

$$\chi'(\Omega_c, \delta, \Delta) \simeq -\frac{N\mu^2}{\hbar\epsilon_0} \frac{4\delta}{\Omega_c^2}. \quad (4)$$

Note that the above approximation is valid as long as  $\Gamma$  is much smaller than  $\frac{\Omega_c^2}{4(\delta^2 + \gamma^2)}\gamma$ . For the cases where we have a

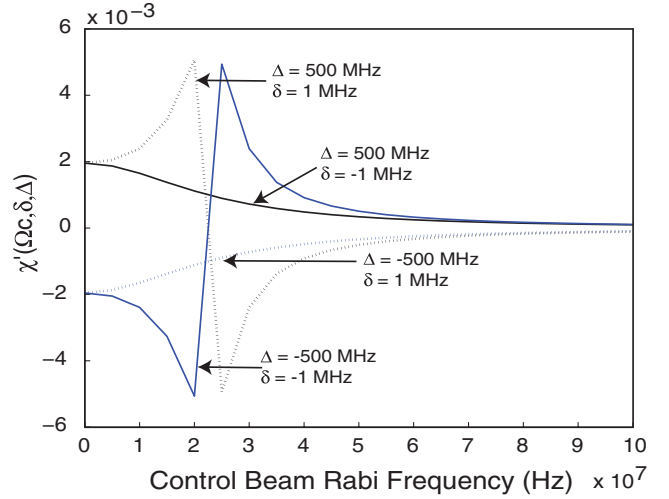


FIG. 2 (color online). The theoretical plot of the real part of the susceptibility as a function of the control beam Rabi frequency. We plot for different signs of two photon detuning and single photon detuning to show the qualitative features of the susceptibility. The parameters  $\delta$  and  $\Delta$  are indicated in the figure for each plot, and  $N$  is taken as  $10^{12} \text{ cm}^{-3}$ .

focused signal or focused coupling beams, a large  $\Gamma$  resulting from the residual Doppler broadening due to angular mismatch of signal and coupling beams is compensated by having higher coupling beam intensities so that the power broadening dominates all other decoherence mechanisms.

We can design the waveguide by choosing appropriate parameters. A donut shaped control beam with  $\Delta$  and  $\delta$  having the same sign results in a refractive index profile analogous to a fiber. One significant difference of this scheme from [10] is that the latter relies on pumping of the population to one of the excited states, which requires much more control beam power (400 mW) than our scheme (20 mW). Even with very large control beam powers, only 50% of the population can be pumped to the excited state, limiting the refractive index difference between “core” and “cladding.” On the other hand, the scheme in [10] guides the signal over wider bandwidth.

The plot showing the transmission of the signal beam as a function of Raman detuning is shown in Fig. 3(a). The control and the signal are tuned to be about 500 MHz to the blue of  $\text{Rb}^{85} F = 2$  to  $F' = (2, 3)$  and  $F = 3$  to  $F' = (2, 3) D_1$  transitions, respectively. Both control and signal are collimated and are copropagating. The dispersion of the medium is obtained by using Kramers-Kronig relations. Figure 3(b) shows the plot of the variation of the refractive index at a fixed signal frequency with a  $\delta = -1.5$  MHz versus control beam power. We can see that the refractive index decreases with increasing control beam intensity. We choose the signal frequency to be close to Raman resonance such that there is good contrast in the refractive index for higher and lower control beam powers and

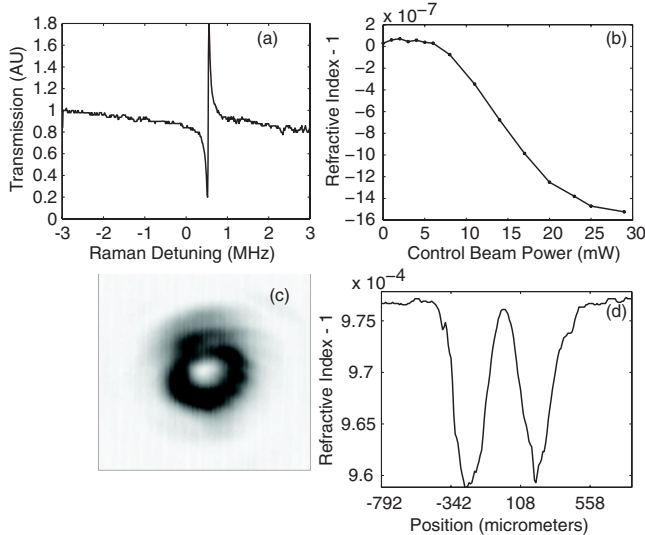


FIG. 3 (color online). (a) shows the experimental plot of the variation in the transmission of signal versus Raman detuning. (b) is the plot of the refractive index of the signal, tuned  $-1.5$  MHz away from Raman resonance, as a function of control beam power. The dotted line in the figure is the experimental data, and the solid line is to guide the eye. (c) shows the spatial variation of refractive index. White indicates higher refractive index and black, along the ring of the donut, is lower refractive index. (d) shows the plot of refractive index versus position along one of the axes. We use a single photon detuning of  $500$  MHz, a Raman detuning of  $-1$  MHz, and  $30$  mW control beam power in Eq. (2) to obtain the refractive index profiles from a camera snapshot of the intensity profile.

away from the absorption dip shown in Fig. 3(a). We found that we have optimum guiding at a  $\delta = -2$  MHz.

Figure 3(c) shows the refractive index profile along the transverse plane. The intensity profile at the front of the vapor cell is captured with a camera and Eq. (2) is used to obtain the refractive index. Figure 3(d) shows the index profile along one of the axes of the beam. We see that we have a refractive index contrast of about  $10^{-5}$  between maximum and minimum refractive indices. Figure 4 shows the results of the experiment. The control beam is converging along the cell and has a focus at the back face of the cell. The signal is focused into the “core” of the control beam at the front face as shown in Fig. 4(c). In the absence of the control beam, the signal beam diverges along the length of the cell as shown by the gray curve in Fig. 4(d). The Gaussian width of the signal at the front face of the cell is  $56 \mu\text{m}$ , and at the back face it is  $102 \mu\text{m}$  without the control beam. When the control is on, the signal is guided along its core, and so the signal beam diameter is smaller at the back face of the cell. For example, the Gaussian width of the signal at the back face is  $35 \mu\text{m}$  with an  $18$  mW input control [black curve of Fig. 4(d)]. The integrated intensity of the black curve is approximately  $43\%$  of the gray curve, implying that there is a good coupling of the signal power into the waveguide. Note that the peak inten-

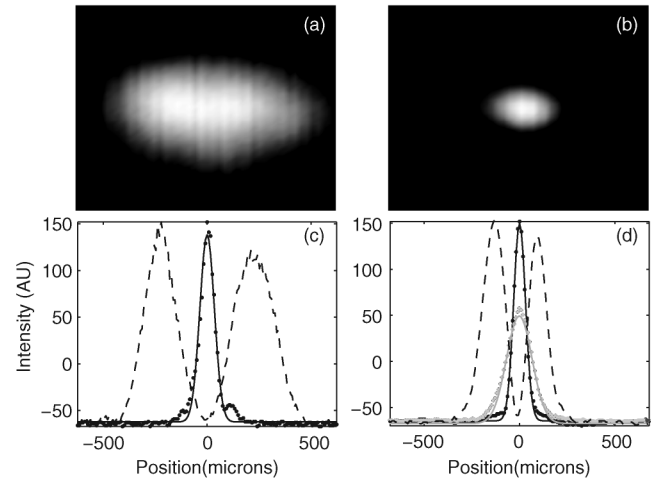


FIG. 4. (a) and (b) are snapshots of the signal beam profile at the back of the vapor cell with the control beam off and on, respectively. The back face of the cell is imaged on to the camera by a  $4f$  imaging system. (c) shows the beam profiles along the longer axis of the beams at the front face of the cell. The dashed line is the measured control beam intensity, the dotted line is the measured signal intensity, and the solid line is the Gaussian fit to the measured signal intensity. The Gaussian width of the signal is  $56 \mu\text{m}$ . The plots in (d) show the beam profiles at the back face of the cell. The black dashed line is the measured control beam profile, the gray and black dotted lines are the measured signal beam profiles when the control is off and on, respectively, and the solid gray and black lines are Gaussian fits to the dotted lines. The Gaussian widths of gray and black curves are  $102 \mu\text{m}$  and  $35 \mu\text{m}$ , respectively. Note that the integrated intensity of the black curve is approximately  $43\%$  of the gray curve, indicating a good coupling of power into the waveguide. The control beam power is  $18$  mW. The control beam intensity in (c) and (d) is normalized to fit in the figure, while the signal intensities in (d) are relative.

sity of the black curve is more than that of the gray curve. The control beam intensity in Figs. 4(c) and 4(d) is normalized to fit in the figure, while the signal intensities in Fig. 4(d) are relative. The laser beams are slightly elliptical, and so the axis mentioned above is along the longer axis. The snapshots of the signal beam with and without the control beam at the back face of the vapor cell are shown in Figs. 4(a) and 4(b).

The size of the signal at the back of the cell also depends on the control beam power, as shown in the Fig. 5(a), and on the two photon detuning, as shown in Fig. 5(b). Figure 5(b) also shows that we can have waveguiding for a range of frequencies to the blue of Raman resonance. This means that we can potentially guide optical pulses with bandwidths of a few megahertz. Figure 5(c) shows the output powers for different frequencies. To verify that the waveguide is linear in signal power, we measure the output signal power for various input signal powers as shown in Fig. 5(d). We see that the plot is linear with a slope of about  $0.43$ , which means that we couple  $43\%$  of input signal

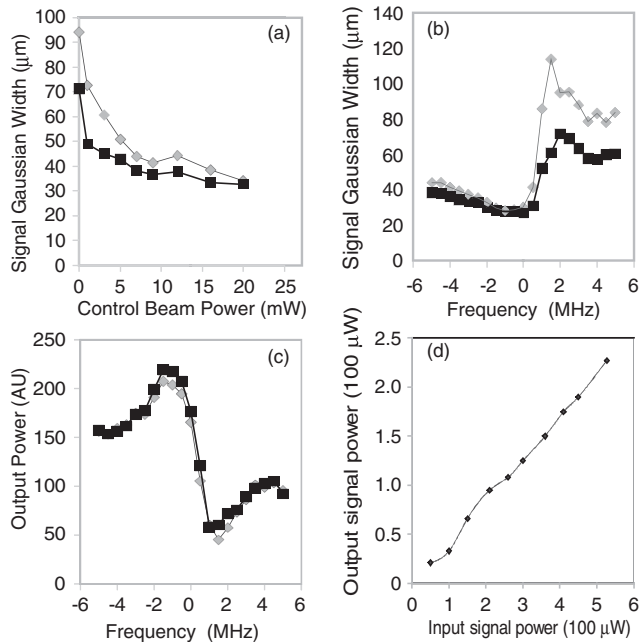


FIG. 5. (a) and (b) are the plots of the signal beam size at the back face of the vapor cell versus the control beam power and Raman detuning, respectively. (c) is the plot of output signal power versus Raman detuning. (d) is the plot of output signal power versus input signal power. The plot is nearly linear; the slope of the linear fit to data is 0.43. In (a), (b), and (c) gray is the measure along longer axis, and black is the measure along the shorter axis of our elliptical beam.

power into the waveguide. This implies that we can expect to guide light of very low power without significant loss.

This all optical waveguide can be used to achieve efficient nonlinear processes at very low light levels. For example, in the case of naturally abundant rubidium, we can use one isotope to guide the signal and the other isotope as a medium for the nonlinear processes such as two photon absorption, Stark shift, Kerr effect, etc. Lukin and Imamoglu [17] suggested the use of rubidium isotopes for two simultaneous, independent nonlinear processes to achieve large Kerr nonlinearities. One can also optimize the waveguide to increase the bandwidth and allow for multiple frequency waveguiding. Finally, one can use this waveguide as a building block for an all optical beam coupler and beam splitter, similar to solid-state waveguide devices.

In summary, we use the intensity dependent refractive index resulting from a Raman transition in a  $\Lambda$  system to create an all optical waveguide. We are able to transmit about 43% of the power along the waveguide, for lengths much greater than the diffraction length, using a low power control beam. This waveguide can be used to achieve efficient nonlinear processes at very low light levels.

We gratefully acknowledge support from DARPA DSO Slow Light, the DOD MURI for Quantum Imaging, and the National Science Foundation.

\*praveen@pas.rochester.edu

- [1] F. Benabid, J.C. Knight, G. Antonopoulos, and P.S.J. Russell, *Science* **298**, 399 (2002).
- [2] S. Ghosh, A.R. Bhagwat, C.K. Renshaw, S. Goh, A.L. Gaeta, and B.J. Kirby, *Phys. Rev. Lett.* **97**, 023603 (2006).
- [3] S.M. Spillane, G.S. Pati, K. Salit, M. Hall, P. Kumar, R.G. Beausoleil, and M.S. Shahriar, *Phys. Rev. Lett.* **100**, 233602 (2008).
- [4] R.R. Moseley, S. Shepherd, D.J. Fulton, B.D. Sinclair, and M.H. Dunn, *Phys. Rev. A* **53**, 408 (1996).
- [5] R.R. Moseley, S. Shepherd, D.J. Fulton, B.D. Sinclair, and M.H. Dunn, *Phys. Rev. Lett.* **74**, 670 (1995).
- [6] D.R. Walker, D.D. Yavuz, M.Y. Shverdin, G.Y. Yin, A.V. Sokolov, and S.E. Harris, *Opt. Lett.* **27**, 2094 (2002).
- [7] D.D. Yavuz, D.R. Walker, and M.Y. Shverdin, *Phys. Rev. A* **67**, 041803(R) (2003).
- [8] M.Y. Shverdin, D.D. Yavuz, and D.R. Walker, *Phys. Rev. A* **69**, 031801(R) (2004).
- [9] N.A. Proite, B.E. Unks, J.T. Green, and D.D. Yavuz, *Phys. Rev. A* **77**, 023819 (2008).
- [10] A.G. Truscott, M.E.J. Friese, N.R. Heckenberg, and H. Rubinsztein-Dunlop, *Phys. Rev. Lett.* **82**, 1438 (1999).
- [11] R. Kapoor and G.S. Agarwal, *Phys. Rev. A* **61**, 053818 (2000).
- [12] J.A. Andersen, M.E.J. Friese, A.G. Truscott, Z. Ficek, P.D. Drummond, N.R. Heckenberg, and H. Rubinsztein-Dunlop, *Phys. Rev. A* **63**, 023820 (2001).
- [13] H. Shpajman, A.D. Wilson-Gordon, and H. Friedmann, *Phys. Rev. A* **71**, 043812 (2005).
- [14] O. Firstenberg, M. Shuker, N. Davidson, and A. Ron, *Phys. Rev. Lett.* **102**, 043601 (2009).
- [15] J.P. Marangos, *J. Mod. Opt.* **45**, 0471 (1998).
- [16] M. Fleischhauer, A. Imamoglu, and J.P. Marangos, *Rev. Mod. Phys.* **77**, 633 (2005).
- [17] M.D. Lukin and A. Imamoglu, *Phys. Rev. Lett.* **84**, 1419 (2000).